Influence of the presence of the heme cofactor on the JK-loop structure in indoleamine-2,3-dioxygenase-1

Mirgaux, Manon; Leherte, Laurence; Wouters, Johan

Published in:
Acta crystallographica. Section D: Structural Biology

DOI:
10.1107/S2059798320013510

Publication date:
2020

Document Version
Peer reviewed version

Influence of the presence of the heme cofactor on the JK-loop structure in indoleamine-2,3-dioxygenase-1

Mirgaux Manon,* Leherte Laurence and Wouters Johan *

Namur Institute of Structured Matter (NISM), Namur Research Institute for Life Science (NARILIS), Department of Chemistry, Laboratoire de Chimie Biologique Structurale (CBS), University of Namur (UNamur), 61 Rue de Bruxelles, 5000 Namur, Belgium. E-mail: manon.mirgaux@unamur.be, johan.wouters@unamur.be

human indoleamine-2,3-dioxygenase-1; **tryptophan metabolism**; **cancer immunotherapy**; **JK-loop conformation**; **Molecular Dynamics**

PDB reference: indoleamine-2,3-dioxygenase-1, 7A62.

Abstract

Indoleamine-2,3-dioxygenase-1 (hIDO1) has sparked an interest in cancer research as an immunotherapeutic target. Its structure includes a loop, named the JK-loop, that controls the orientation of the substrate or the inhibitor within the active site. However, little has been reported about the crystal structure of that loop. For the first time, in the present work, the conformation of the JK-loop is determined in the presence of the heme cofactor in the active site through X-ray diffraction experiments (2.44 Å). Molecular Dynamics trajectories are also carried out to provide a dynamical information about the loop according to the presence of cofactor. Such new structural and dynamical information highlights the importance of the JK-loop in confining the labile heme cofactor into the active site.

1. Introduction

Due to its degradation into numerous bioactive metabolites, L-Tryptophan (L-Trp) is the less abundant but essential amino acid in mammals (Badawy, A., 2017; Nienhaus, K. *et al.*, 2018; King, N. J. C. *et al.*, 2007). Although the catabolism of L-Tryptophan occurs along four possible pathways, the main way to transform L-Trp is the kynurenine pathway (KP), allowing the transformation of 95% of the L-Tryptophan available from food (Phillips, R. S. *et al.*, 2019). Through KP, L-Trp is converted into L-kynurenine to produce essential metabolites such as redox cofactors, neuroprotectors and neurotoxics (Kolodziej, L. R. *et al.*, 2011). As a result, the KP pathway confers to L-Trp a central role in many diseases, including disruption of the immune response (Cancer, HIV) and neurological disorders (Alzheimer's disease, Parkinson's disease or Huntington's disease) (Munn, D. H. *et al.*, 2013; Mellor, A. L. *et al.*, 2017; Phillips, R. S. *et al.*, 2019). Therefore, enzymes of the kynurenine pathway can be considered as a set of therapeutic targets.

Human Indolenamine 2,3-dioxygenase-1 (hIDO1) and human Tryptophan 2,3-dioxgenase (hTDO) are two heme-containing enzymes that are responsible for the initial as well as the rate-limiting step of the kynurenine pathway (Raven, E. L, 2017). First mentioned in 2018 by Nelp *et al.* (Nelp, M. *et al.*, 2018) and subsequently supported by Pham *et al.* (Pham, K. N. *et al.*, 2019), this heme cofactor is labile in hIDO1. Using a molecule of O_2, hIDO or hTDO transforms L-Trp into N-formylkynurenine (NFK) by an oxidative cleavage of the C2-C3 double bond in the indole moiety (Fig. 1). As hIDO and hTDO are expressed in human tumors, this reaction step has raised an interest in the cancer research, particularly in cancer immune escape and in the resistance to immunotherapy (Uyttenhove, C. *et al.*, 2003; Moon, Y. W. *et al.*, 2015; Takikawa, O., 2005; Prendergast, G. C. *et al.*, 2018; Hoffmann, D. *et al.*, 2019). The induction of

hIDO1 is controlled, among others, by interferons (α, β and γ) which induce inflammatory signals. Therefore, while hTDO catabolizes excess dietary L-Trp to maintain metabolites level, hIDO1 regulates immunity by deactivating T cells. Overexpression of hIDO1 results in local depletion of L-Trp and accumulation of L-kynurenine in the extracellular compartment, which exerts an immunosuppressive response by decreasing T cells activation (Uyttenhove, C. *et al.*, 2003; Mellor, A. L. *et al.*, 2004; Munn, D. H. *et al.*, 2007; Katz, J. B. *et al.*, 2008; Prendergast, G. C., 2008; Moon, Y. W. *et al.*, 2015; Munn, D. H. *et al.*, 2016). Over the years, hIDO1 inhibitors have been developed and tested in clinical trials (Indoximod, Epacadostat, PF-06844003, Navoximod and Linrodostat) (Moon, Y. W. *et al.*, 2015; Prendergast, G. C. *et al.*, 2018). Nevertheless, the recent failure of Epacadostat in phase III of the clinical trials suggests that inhibition of hIDO1 alone is not sufficient to solve the problem of immune escape (Prendergast, G. C. *et al.*, 2018; Pham, K. N. *et al.*, 2019; Long, G. V.. *et al.*, 2019; Peng, Y.-H. *et al.*, 2020) and triggers a revision of the enzyme functioning. Indeed, it is recognized that there is a lack of information on hIDO1, which is necessary to design new inhibitors.

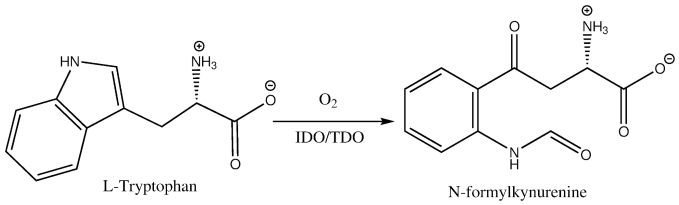

Fig. 1. First step of the kynurenine pathway. Degradation of L-Tryptophan into N-formylkynurenine using hIDO or hTDO.

Since the publication of the two first structures of hIDO1 by Sugimoto *et al.* in 2006 (Sugimoto, H. *et al.*, 2006), many structures of hIDO1 with L-Trp or different inhibitors have been deposited to the PDB (Tojo, S. *et al.*, 2014; Peng, Y.-H. *et*

al., 2016; Wu, Y. *et al.*, 2017; Crosignani, S. *et al.*, 2017; Lewis-Ballester, A. *et al.*, 2017; Lewis-Ballester, A. *et al.*, 2018; Nelp, M. *et al.*, 2018; Alexandre, J. A. C. *et al.*, 2018; Luo, S. *et al.*, 2018; Pham, K. N. *et al.*, 2018; Kumar, S. *et al.*, 2019; Zhang, H. *et al.*, 2019; Pham, K. N. *et al.*, 2019; Rohrig, U. F. *et al.*, 2019; Peng, Y.-H. *et al.*, 2020; White, C. *et al.*, 2020). Particularly, recent improvements involving surface mutations allowed the generation of high-resolution structures (from 1.7Å to 2.7 Å) soaked with L-Trp or inhibitors (Luo, S. *et al.*, 2018). So far, only few articles focus on an in-depth analysis of structural aspects of hIDO1 (Pham, K. N. *et al.*, 2019; Lewis-Ballester, A. *et al.*, 2018; Pham, K. N. *et al.*, 2018; Lewis-Ballester, A. *et al.*, 2017; Sugimoto, H. *et al.*, 2006).

As already mentioned, the JK-loop is very likely involved in the closure of the active site, so that it plays a key role in the inhibition of the enzyme. However, the loop structure has not been fully resolved yet, especially its N-terminal part. The C-terminal part is better resolved and, according to its conformation, the JK-loop structures can be classified in three categories (Supporting Information, Fig. SI1): a closed conformation (PDB codes: 6PZ1, 6E46, 6E35, 6CXU, 6CXV, 5WHR, 6F0A, 5WMU, 5WMV, 5WMW, 5WMX), an intermediate conformation (PDB codes: 6E43 (B), 5ETW (A), 5EK2 (B), 5EK3 (B)) and an open conformation (PDB codes: 6E40 (D), 6E41, 6E42 (D), 6E44 (B), 6E45 (B)). Molecular Dynamics simulations carried out by Alvarez and coworkers also show that the JK-loop is composed of a fixed C-terminal and a more flexible N-terminal part, and they observe the existence of the three interconvertible conformations of the C-terminal component (Álvarez, L. *et al.*, 2016). In parallel, the authors suggest that the N-terminal part may play a role in protein-protein interaction or in post-translational modifications, and highlight its possible role in immune regulation of hIDO1 by regulating its activity.

In the present study, we experimentally determine structural properties of hIDO1 using a ferrous hIDO1 crystal structure at a medium resolution level (2.44 Å). The structure consists of a heme-linked hIDO1 enzyme with a complete JK-loop. Coupled with Molecular Dynamics simulations, the present work provides information on the JK-loop conformation, but also on its dynamics as a function of the presence of the cofactor heme. Such information is essential for a better understanding of the catalytic and inhibition mechanisms for this drug target.

2. Material and methods

2.1. Expression, purification and crystallisation

The human IDO1 gene was expressed using a plasmid pET-28a provided by Tong *et al.* (Luo, S. *et al.*, 2018). The plasmid, containing the His-tagged protein with two surface mutations (K116A, K117A), was transformed into *Escherichia coli* BL21(DE3) cells. The cells were grown in a lysogeny broth (LB) medium supplemented with 50 μg/mL of kanamycin at 37 °C until the culture reaches an optical density of 0.6 at 600 nm. The induction occurs by addition of 0.4 mM of isopropyl-β-D-1-thiogalactopyranoside and 0.75 mM of 5-aminolevulinic acid during 20 hours at 18 °C. Cells were harvested by centrifugation at 4500 rpm for 30 min. Pellets were resuspended in lysis buffer (50 mM Tris base/HCl pH 8.0, 500 mM NaCl, 20 mM imidazole, 5% (v/v) glycerol) supplemented with protease-inhibitor cocktails (cOmplete EDTA-free, one tablet per 50 ml of solution from Roche) and lysed by sonication on ice. Cellular debris were removed by centrifugation at 12 500 rpm for 1 hour. The lysate was filtered on 0.2 mm filter (Whatman, GE Healthcare) and purified by immobilized metal affinity chromatography (IMAC) using an HisTrap FF Crude column (GE Healthcare). After washing of the flow through with buffer A (50 mM Tris base/HCl pH 8.0, 500 mM NaCl, 20 mM imidazole, 5% (v/v) glycerol), the elution occurs using

a gradient of 30 min (0% to 100%) in buffer B (50 mM Tris base/HCl pH 8.0, 500 mM NaCl, 500 mM imidazole, 5% (v/v) glycerol). Reddish fractions containing pure hIDO1 were collected. The purity was followed by 12% SDS-PAGE stained using Coomassie Blue.

2.2. Crystallization assay

After exchanged into a crystallization buffer containing 5mM of HEPES/NaOH pH 7.6, 200 mM NaCl and 5 mM DTT, the protein was concentrated using amicon with a 10 kDa molecular-weight cutoff membrane to reach a concentration of 16 mg/ml. Crystallization assays were carried out with the hanging-drop vapor-diffusion method at 293 K. The wells contained a solution made of 14% of polyethylene glycol 3350 and 0.1M in KH_2PO_4/NaOH at a pH of 6.25. Drops were made with 1 μL of the well solution and 1 μL of the protein solution. Red crystals appeared within one day. Before data collection, crystals were soaked for 2 min with the well solution supplemented with a cryo-solution at a final concentration of 20% of glycerol and 20 mM of sodium dithionite. Sodium dithionite allowed the reduction of the heme iron into the ferrous state. Subsequently, the crystals were flash-cooled in liquid nitrogen.

2.3. X-ray data collection and model refinement

The diffraction data were collected at 100 K at the PROXIMA-1 beamline of the SOLEIL synchrotron (Gif-sur-Yvette, France) using PIXEL detector (DECTRIC EIGER X 16M), at the single wavelength of 0.979 Å for 3600 pictures. The data processing was achieved with the *XDS* program (Kabsch, W., 2010). The structure was solved by molecular replacement performed by *Phaser* (McCoy, A. J. *et al.*, 2007) with a monomer from the PDB entry 6e43 as the model (Luo, S. *et al.*, 2018). The model building and structure refinement were performed using *Coot* (Emsley, P. *et al.*, 2010)

and *PHENIX* (Adams, P. D. *et al.*, 2010) under NCS restraint on torsion-angles. Anisotropy in the data was removed using the extension Morph model on Phenix (Terwilliger, T.C., 2012). The heme cofactor was added to the monomers using Elbow (Moriarty, N.W. *et al.*, 2009). Data collection and refinement statistics are summarized in Table 1. The cavity volumes in the active site were calculated using the POCASA 1.1 server with a grid of 1 Å and a probe radius of 1.0 Å using the chain C of the crystal structure. For visualization purposes, all Figures were generated using *PyMOL* (Schrödinger, LLC, 2010).

2.4. Molecular Dynamics

Molecular Dynamics (MD) simulations of the apo-form of hIDO1 and hIDO1 bound to the heme cofactor were run using the program GROMACS 5.1.4. (Abraham, M. J. *et al.*, 2016) with the CHARMM27 force field (FF) (MacKerell Jr, A. D. *et al.*, 2000) and the CMAP corrections for the protein. The monomer C of the crystal structure (PDB entry: 7A42) was used as starting model. For the simulation without the heme cofactor, the construction of the model was performed by removing the heme group of the chain C of the crystal structure. A RMSD analysis between the chain and the monomers of the apo-forms reported in the PDB yields values of 0.3 Å for the structure 6E43, 0.5 Å for 6AZV, and 0.6 Å for 6AZW. These RMSD values are low enough to consider the unbound chain C of 7A62 as a model of the apo-form of the enzyme. H atoms were added using GROMACS. To reduce the calculation time, the systems were solvated using all-atom TIP3P and coarse-grained SIRAH water particles (Darré *et al.*, 2012; Gonzalez, H.C.*et al.*, 2013; Leonardo *et al.*, 2015). A cubic box was built around the protein with at least 2.0 nm between the box and the protein atoms. TIP3P water molecules were placed in a shell of 1.0 nm thickness around the molecular system. Then, the space between the shell and the box was completed with

coarse-grained SIRAH water particles. The use of a hybrid all-atom/coarse grained water solvent allows to model a protein system which remains fully surrounded by all-atom water molecules as illustrated in Supporting information, Fig. SI2. Finally, the total charge of the system was neutralized with sodium ions randomly placed in the bulk of the SIRAH water particles.

The optimization and MD trajectories were generated under the particle mesh Ewald (PME) periodic boundary conditions (PBC). A cut-off value of 1.2 nm was applied for Coulomb and Van der Waals interactions. Temperature and pressure were fixed using the Parrrinello-Rahman (Parrinello, M., *et al.*, 1981) and V-Rescale algorithms (Bussi, G. *et al.*, 2007), respectively. Covalent bonds involving hydrogen atoms were constrained using the LINCS algorithm (Hess, B. *et al.*, 1997). The resulting system was optimized using the steepest descent algorithm for a maximal number of 2500 steps and an initial step size of 0.05 nm. During the equilibration stage of the system, the temperature was progressively increased from 50 K to 310 K using short MD runs. The first run consisted of a 10 ps simulation at 50 K on the system obtained after optimization. Afterwards, the system was relaxed for two runs of 20 ps at 150 K and 310 K. Finally, a run of 50 ps at 310 K and 1 bar was performed to finalize the relaxation of the system. The equilibration was extended during 60 ns with a time step of 2 fs at 310 K and 1 bar. The production step was ran for 200 ns (100×10^6 steps) with a time step of 2 fs. The evolution of the system during the equilibration and the production stages was followed using energy and RMSD (Root mean square displacement) profiles. The calculation of the RMSD and RMSF (Root mean square fluctuation) profiles were achieved using the initially optimized protein structure as the reference structure, which presents an RMSD of 0.2 Å in comparison to the crystal structure.

3. Results and discussion

3.1. Overall structure

The hIDO1 crystals obtained with the vapor-hanging-drop method belong to the $P2_12_12$ space group, and the unit cell parameters are a=80.96 Å, b=117.95 Å and c=216.41 Å. The heme-bound hIDO1 crystal structure is composed of four monomers (A, B, C, D) with missing atoms at the extremities. More precisely, in monomer A, the protein is refined from the amino acid S12 to K401, while in monomers B and C the structure includes the amino acid G11 to G403. Finally, in monomer D, the amino acids G11 to K401 are refined. The residues that are located at the N-terminal extremity of the JK-loops, i.e., from P362 to T379 in A and D, and from P362 to G378 in B, are not refined. Contrarily, the JK-loop of monomer C is fully resolved, leading to a complete structure of the loop ever reported. The superposition of the four monomers gives the following RMSD between A-B (0.123 Å), A-C (0.239 Å), A-D (0.226 Å), B-C (0.236 Å), B-D (0.216 Å), and D-C (0.139 Å). The mean RMSD value between each monomer of the crystal structure and their corresponding monomer from the literature gives a value of 0.29 ± 0.012 Å (PDB entry : 6e45 (Luo, S. *et al.*, 2018)).

In the structure, each monomer is composed of two domains, i.e., the small domain considered as the N-terminal moiety and the large domain consisting in a bundle of 13 α-helices (Fig. 2, (a)). The largest domain includes the catalytic core formed by the heme cofactor and the α-helices B and D, this latter being part of the DE-fragment which closes the active site together with the JK-loop (Q360 to G380). Indeed, the DE-fragment is composed of the α-helix D (N222 to V229), the DE-loop (L230 to S263) and two 3_{10}-helices (N240 to S244 and S263 to V269). In this general organization, an additional 3_{10}-helix built from R296 to M299 occurs in the monomers A and B. Pre-α-helix D, and the BC- and HI-loops are involved in dimerization in the crystal structure. A parallel β-sheet comprised between V102-L103 and V248-Y249 in the DE-

fragment binds both domains (black circle, Fig. 2, (b)). The small domain contains the residues G11 to D158. It is made of six α-helices (involving amino acids Y36 to H45, H45 to S52, Q54 to K61, D72 to G93, P104 to E119, and V125 to V130, or helix A, contributing to the active site), four 3_{10}-helices (S12 to H16, P33 to F35, S66 to L70, and T144 to E146), and a small anti-parallel β-sheet formed by the amino acids K135-K136 and M148-D149 (Fig. 2, (b)).

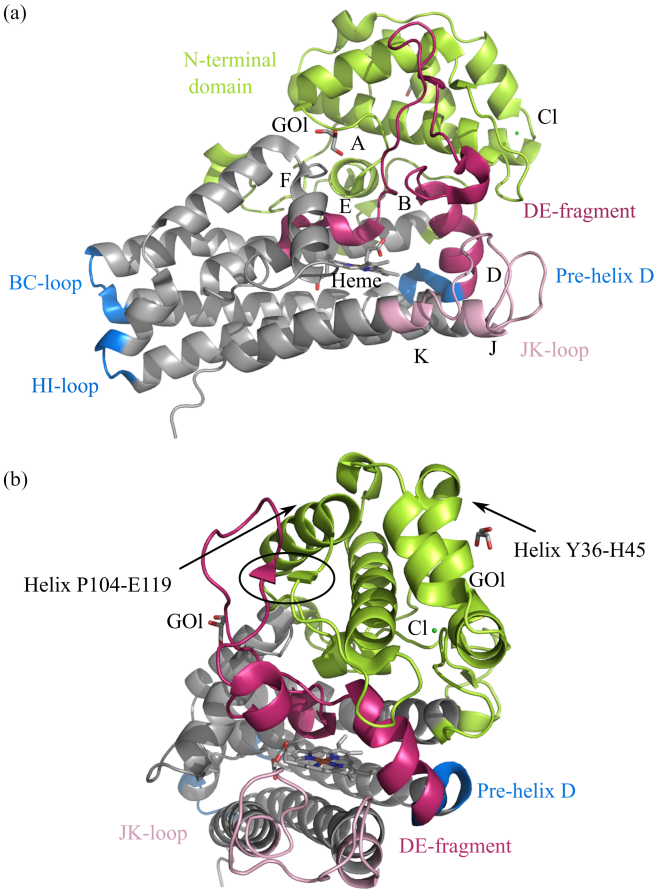

Fig. 2. (a) Crystal structure of monomer C. Small and large domains are in green and grey, respectively. In the large domain, the pre-helix D, BC-loop, and HI-loop, are coloured in blue. The DE-fragment is in magenta, and the JK-loop is represented in light pink. (b) Lateral view of the small domain showing the helices P104 to E119 and Y36 to H45. A β-sheet links the small and the large domain (black oval).

3.2. Quality of the refined structure

The heme-bound hIDO1 structure is solved at a resolution of 2.44 Å, with R_{work} and R_{free} equal to 0.2118 and 0.2579 respectively. Seven glycerol molecules and two chloride ions are also present in the structure. The Ramachandran plot, obtained using MolProbility (Chen *et al.*, 2010), shows that 96 % of the residues adopt allowed Φ-Ψ values, and only 0.33 % are reported as outliers in the structure. Rotamers outliers amount to 1.3 %. Since most of these outliers are located in the JK-loop, their conformation variability highlights a greater flexibility. Statistics for the refined model (bond lengths and bond angles RMSD values) stress a good quality of the structure. The crystal structure has an overall B-factor of 39.83 $\mathring{A}^2$. Particularly, residues Q360 to G380 are characterized by the largest B values in each monomer (Fig. 3). It reflects the enhanced dynamics of the protein residues around the JK-loop.

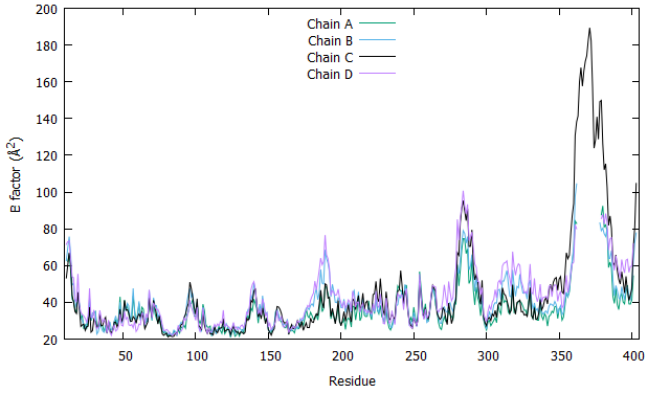

Fig. 3. B-factor ($\mathring{A}^2$) profile of the residues main chain for each monomer.

Table 1. *Data collection and refinement statistics for crystal structure. Values in parentheses are for the highest resolution shell.*

PDB code	7A62
Data collection	
Beamline	SOLEIL - PROXIMA-1
Wavelength (Å)	0.979
Resolution (Å)	49.18-2.438 (2.525-2.438)
Space group	$P2_12_12$
a, b, c (Å)	80.96 117.95 216.41
α , β, γ (°)	90 90 90
Total reflections	1067214 (93823)
Unique reflections	77982 (4879)
R_{merge}	0.1677 (1.828)
R_{meas}	0.1742 (1.907)
$CC_{1/2}$	0.998 (0.753)
CC*	1 (0.927)
I/σ (I)	8.81 (0.84)
Completeness (%)	84.0 (98.0)
Multiplicity	13.7 (12.4)
Wilson B-factor ($\AA^2$)	38.98
Refinement	
No. of reflections	65724 (4878)
No. of reflection used for R_{free}	3301 (255)
R_{work}	0.2118 (0.3717)
R_{free}	0.2579 (0.4351)
CC(work)	0.941 (0.665)
CC(free)	0.923 (0.745)
No. of non-hydrogen atoms	
Total	12873
Protein	11962
Ligands/ions	216
Protein residues	1533
B factors ($\AA^2$)	
Overall	39.83
Protein	39.71
Ligands/ions	45.98
Water	40.14
R.M.S deviations	
Bond lengths (Å)	0.014
Bond angles (°)	1.05
Ramachandran plot	
Favored (%)	96
Allowed (%)	3.7
Outliers (%)	0.33
Rotamers outliers (%)	1.3
Clash score	6.46

3.3. Description of the dimerization interface

While hIDO1 functions as a monomer in the biological state, the hIDO1 unit cell of the crystal structure contains four molecules per asymmetric unit. On the whole, the four hIDO1 molecules of an asymmetric unit are interconnected and can be considered as a dimer of dimers. Translation and inversion operations appear between the dimers A/D and B/C. Alignment of the two dimers results in a RMSD of 0.26 Å. Such a crystal packing results in multiple monomer/monomer interfaces in both the small and large domains of the protein. In the small domain, mutations such as K116A and K117A allow the alignment of α-helix P104-E119 of monomer A with the same helix of monomer D of a contiguous asymmetric unit, and inversely (Fig. 4, (a)). Similar interface occurs between monomers B and C. The A/D (D/A) and B/C (C/B) dimers involve hydrophobic effect triggered by an apolar cluster containing residues V109, F252 and W253 in one monomer, and A116 and A117 in the partner monomer (magenta boxes in Fig. 4, (a)). Electrostatic interactions also occur between residues E119/K257, with distance values of 3.6 Å (green boxes in Fig. 4, (a)). In addition, both residues Q113 of a dimer interact with each other through weak hydrogen bonds (the acceptor-donor distances range from 3.6 Å to 3.9 Å). The helix S66 to L70 strengthens the dimerization through electrostatic interactions between D68 of one monomer and R109 in the other monomer (distance is equal to 3.9 Å). Chalcogens interactions are also observed between the electrophilic sulfur atoms of M64 and the nucleophilic carboxylate oxygen atoms of D68 (distance values between 3.6 Å and 3.9 Å) (orange boxes in Fig. 4, (a)) (Iwaoka, M. *et al.*, 2015; Pal, D. *et al.*, 2001). Selected distances are provided in Supporting information (Table SI1). The small domain also contains a second dimerization site that is located in the neighborhood of the α-helix Y36 to H45 and Q54 to K61 (Fig. 4, (b)). Helix Y36 to H45 and residue R58 of monomer A and B dimerize with α-helix Q54 to K61 of monomer D and C, respectively. The

stabilization occurs using hydrogen bonds (acceptor-donor distances between 2.1 Å and 3.6 Å), electrostatic interactions involving R58, E57 and K61 (bond-lengths distances between 2.2 Å and 4.2 Å), a π-cation interaction between F41 and R58 from the next asymmetric unit (distance value of 3.9 Å, angle of 70.5 degrees with respect to aromatic cycle) strengthened by a displaced parallel π-π interaction between F41 and H45 (distance of 4.3Å between the two centroids).

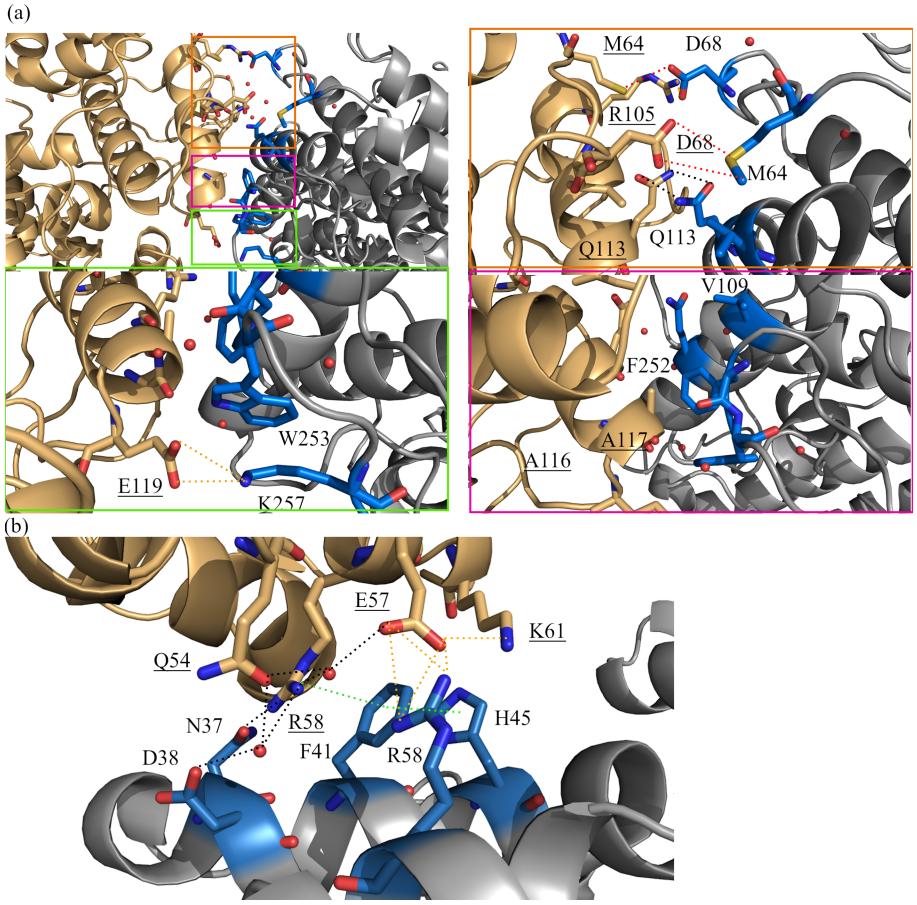

Fig. 4. Small domain dimerization interface between the monomer A of the reference crystal structure (gray) and the monomer D of the surrounding asymmetric unit (gold). The amino acids of the crystal structure involved in the dimerization are in blue. The labels of the residues of monomer D are underlined. Hydrogen bonds, electrostatic, and chalcogen interactions are shown with black, orange, and red dotted lines, respectively. (a) Global view and zooms of the dimerization interface containing the α-helix P104-E119 and the fragment S66 to L70. (b) Dimerization interface with α-helix Y36 to H45, R58 and α-helix Q54 to K61.

The large domain of the enzyme presents three dimerization sites involving the pre-α-helix D, BC-loop, and HI-loop. All of the distances calculated between the monomers are listed in the Supporting Information (Table SI2). The pre-α-helix allows the dimerization of monomers A/D and B/C inside a single asymmetric unit (Fig. 5, (a)). Monomer/monomer interactions by ions pair, already described in other proteins (Birktoft, J. J., 1983; Shankar, B. G. *et al.*, 2007), appear between H218 of A and D219 of D, with distance values between 3.4 Å and 4.9 Å. Hydrogen bonds involving water molecules strengthen the interface and are characterized by distances between 2.2 Å and 3.8 Å. The BC-loop and HI-loop of monomer A and B interact with the equivalent loop of the monomers C and D from a contiguous asymmetric unit respectively (Fig. 5, (b)). These interactions (A/C, B/D, C/A and D/B) are conducted through ions pair and hydrogen bonds networks. In particular, strong electrostatic bonds involve R193 and D325 of both monomers (distance between 2.5 Å and 4.7 Å). Interactions between Q191 and K323 also participate to the asymmetric unit organization.

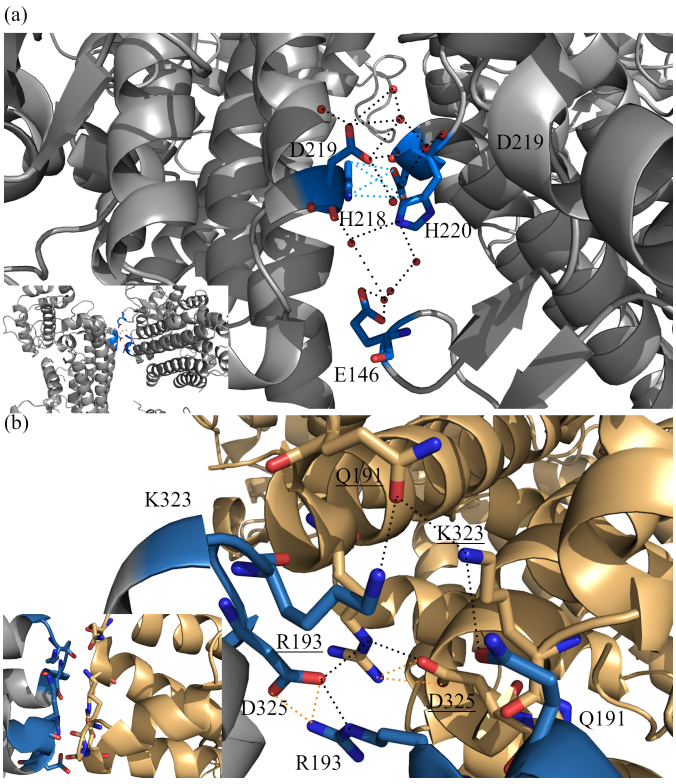

Fig. 5. Large domain dimerization interface between the monomer A of the reference crystal structure (gray) and the monomer of the surrounding asymmetric unit (gold). The amino acid of the crystal structure involved in the dimerization are in blue. The labels of the residues of monomer of the surrounding asymmetric unit are underlined. Hydrogen bonds, electrostatic, and ion-pair interactions are shown with black, orange, and blue dotted lines, respectively. (a) Dimerization interface A/D within a single asymmetric unit involving the pre-α-helix D. (d) Dimerization interface between A/C involving the BC- and HI-loops.

The structures from Luo *et al.* (PDB codes 6E40, 6E41, 6E42, 6E44, 6E45 and 6E46 (Luo, S. *et al.*, 2018)) are the most similar ones to our structure, as far as the crystal organization is concerned. Nevertheless, slight differences exist in the symmetry operations between the monomers of the asymmetric unit, leading to a high RMSD. In the literature, hIDO1 is reported to be a monomeric enzyme. However, the analysis of different crystal packings allows a sampling of possible conformations. In the crystal structures, dimeric interfaces stabilize the JK-loop, the C-terminal part being involved in more interactions than the N-terminal part of the loop. These inter-

faces involve the J- and K- α-helices, the H45-S52 α-helix (Supporting information, Fig. SI3, (a)), and the Q54-K61 α-helix (Supporting information, Fig. SI3, (b)) from the next asymmetric unit. Weak interactions contribute to the organization of the N-terminal part of the loop, in particular hydrogen bonds involving Q348/R58, T351, and water molecules, as well as close contacts between F41/S359 and L49/I356. In contrast, amino acids of the K α-helix are involved in strong electrostatic interactions (D48/K389, E51/E392, E51/K397, R56/E401 and K94/E396) and contribute to a dense hydrogen bond network (S52/R392/K94/water and R56/E401/water), and a chalcogen interaction between D48 and M385. Resulting from these interfaces, the C-terminal part of JK-loop is more stable leading to better refinement of this extremity in contrast to the N-terminal part that remains unclear. In the present crystal structure, an empty space is generated through the crystal packing close to the JK-loop allowing a less constrained conformation (Supporting information, Fig. SI4). Nevertheless, in the same way as observed for the C-terminal extremity in other structures of hIDO1, the stabilization of the pre-α-helix D close to the N-terminal part of the JK-loop facilitates the refinement of this part of the loop. Differences in crystal packings thus allow the observation of distinct structural features on the protein surface. It highlights the importance of analyzing polymorphism during protein refinement and justifies the study of alternative crystal forms to provide a more detailed structural picture of a protein.

3.4. Conformation of JK-loop

In the crystal structure reported here, a fully refined JK-loop is obtained for the monomer C. It allows a better understanding of the enzyme structure. Quality of the electron density for that region of the protein is still poor but all heavy atoms of the main chain of the JK-loop could be traced and refined for the first time. The

N-terminal end of the loop (residues Q360-L374) is still very flexible, as confirmed by high B factors (Fig. 6, (a)) and the electron density distribution remains unclear for some lateral chains and for residue S372. However, overall, the electron density distribution for most of the main chain of the loop is defined. Most residues of the C-terminal part of the JK-loop (E375-G380) are defined (Fig. 6, (a) and (b)) except for A376. The refined JK-loop adopts a conformation between the intermediate and the fully extended ones. The C-terminal part of the loop interacts with the heme moiety through electrostatic interactions with K377 (Fig. 6, (b)) at 4.3 Å and 5.1 Å between the residue and the carboxylate of the cofactor. Compared to what is observed in other available crystal structures, the conformation of the JK-loop presented here is new although close to the one reported by Luo *et al.* (6E41, 6E42, 6E44 and 6E45) (Luo, S. *et al.*, 2018). In the present crystal structure, the JK-loop completes the α-helix K with a supplementary turn. This conformation of the JK-loop prevents the orientation of T379 and G380 into the active site, while residue K377 interacts with the heme cofactor. Consequently, the C-terminal part is oriented towards the active site, in an opposite way to the opened conformations of Luo *et al.* Because of this overall conformation, the pocket A is not open in the crystal structure due to a movement of residues 262-265, as there is no ligand. The same can be observed in other published IDO1 X-ray structures. The pocket B is formed within the free space between the DE-fragment and the JK-loop (Fig. 6, (c)) and allows the entrance of a L-Trp into the enzyme (volume of 249 $\AA^3$, as calculated with POCASA 1.1 server) (Yu, J. *et al.*, 2010) (Supporting information, Fig. SI5). As previously mentioned, the JK-loop may play a role in the regulation of the enzyme activity. Indeed, the conformation of this loop may help the protein to regulate the entrance of L-Trp into the active site and thus its degradation, while maintaining the heme moiety inside the active site through interactions with residue K377.

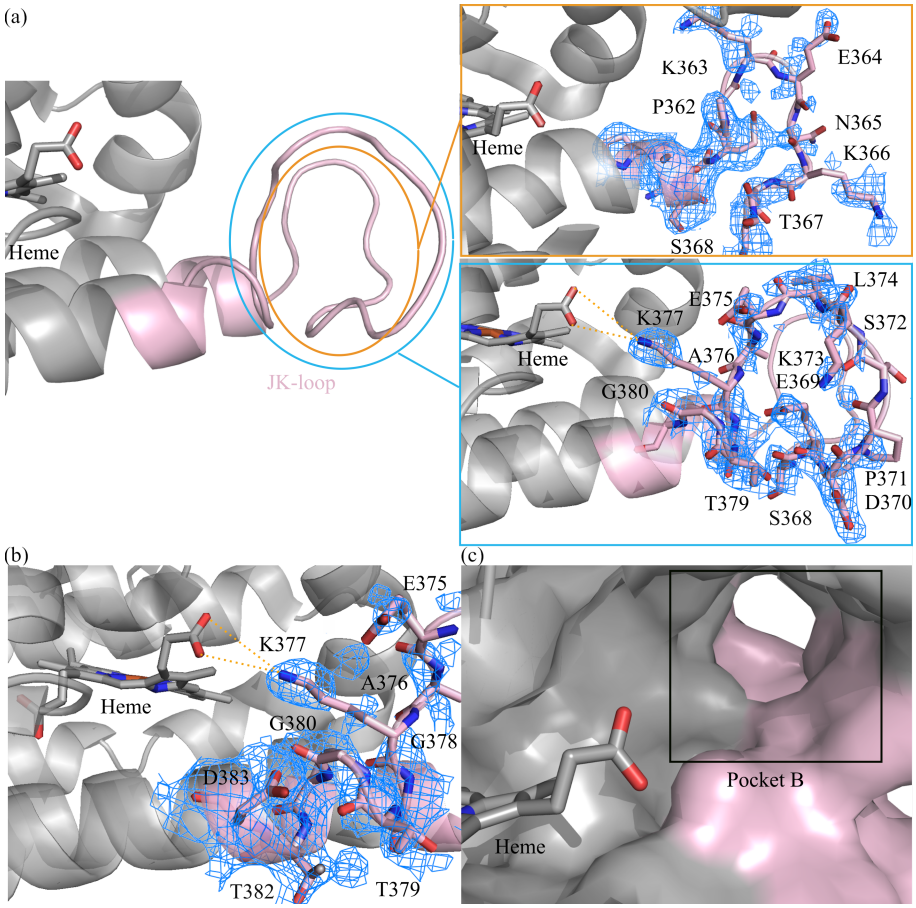

Fig. 6. Conformation of the JK-loop in crystal structure. The 2Fo-Fc map around the residues is represented at 0.5 σ (blue mesh), only density of interest in drawn for clarity. (a) Density around N-terminal part (residues Q360 to L374) represented in two levels: amino acid from Q360 to S368 in orange and amino acid from S368 to L374 in blue. (b) Density around the JK-loop in the C-terminal part. Interaction of K377 with the carboxylate function of heme moiety in orange. (c) Pocket B resulting in the active site.

3.5. Link between JK-loop conformation and heme lability supported by Molecular Dynamics

While Alvarez and coworkers (Álvarez, L. *et al.*, 2016) studied the dynamics of the whole protein in presence of L-Trp, the MD calculations reported here focus on the JK-loop conformation changes in the presence or in the absence of the heme cofactor. In order to investigate the dependence of the JK-loop conformation on the heme group,

MD simulations were performed with and without the cofactor. In the simulation with the cofactor, this latter remains free to move in order to be consistent with its reported lability (Nelp, M. *et al.*, 2018; Pham, K. N. *et al.*, 2019). During production stage, simulations illustrate the independence of the C-terminal extremity of the JK-loop in relation to the N-terminal extremity. The simulated conformations present only slight difference at the level of the C-terminal part of the loop with the cofactor compared to the crystallographic structure (Fig. 7, (b) and Supporting information, Fig. SI6, (b)). The differences between the simulations without the cofactor and the crystallographic structure are more significant (Fig. 7, (b) and Supporting information, Fig. SI6, (b)). Contrarily, the N-terminal part adopts two totally different conformations during the MD simulations (Fig. 8, (a) and Supporting information, Fig. SI6, (c)). The RMSD and RMSF analyses (Fig. 7, (a), (b) and (c)) confirm that the JK-loop has a significant dynamical character as recorded in experimental structures.

The conformation of the C-terminal part of the loop (considered between E375 and G380) is linked to the presence of the heme cofactor. In presence of the heme cofactor, lysine K377 is oriented towards the active site. The average distance between K377 and the carboxylate of the heme cofactor amounts to 6.8 Å ± 2.4 Å and 6.9 Å ± 2.4 Å. To characterize the JK-loop opening as a function of the presence of the cofactor, the distance between K377 and A264, located above the heme moiety, is chosen as a criterion. In the simulated structure with the heme cofactor, the mean distance between the atoms CB of A264 and NZ of K377 amounts to 12.5 Å ± 2.3 Å. The standard deviation highlights a variability in the location of the lysine K377 (Supporting Information, Fig. SI7). In comparison to previous results reported in the literature by Alvarez and coworkers (Álvarez, L. *et al.*, 2016), the most recurrent conformation of the JK-loop in the C-terminal extremity can be considered as an intermediate conformation (Fig. 7, (d)). In the absence of the heme cofactor, K377

is oriented towards the solvent with the amine group pointing towards the outside of the enzyme. Without the heme moiety, the distance between the atoms CB of A264 and NZ of K377 considerably increases to 25.5 Å ± 1.3 Å (Fig. 7, (d)). Thus, this displacement of K377 is seen as a stage that initiates the opening of the JK-loop.

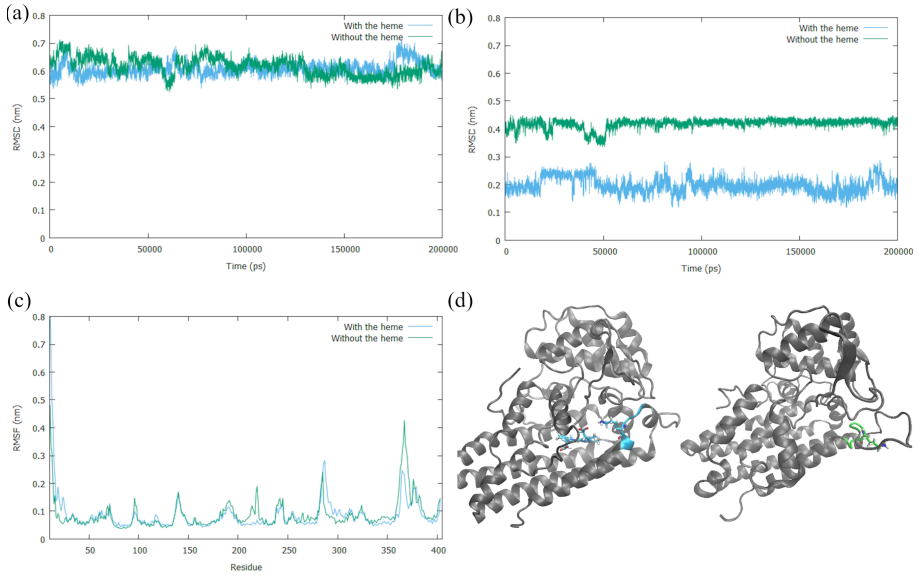

Fig. 7. Impact of the heme cofactor on the JK-loop conformation (with the cofactor (cyan), without the cofactor (green)). RMSD (a) and RMSF analysis (b) of the JK-loop according to the cofactor occupancy. (c) RMSD of the C-terminal part of the JK-loop according to the cofactor occupancy (d) Conformation of the JK-loop on the C-terminal part according to the presence of the heme cofactor. Opening of the JK-loop illustrate with the heme (left) and without the heme (right) as obtained from 200 ns of MD simulation at 300 K and 1 bar.

Regarding the N-terminal part (Q360-L374), the MD simulations support the high flexibility of this part of the loop as illustrated by the larger RMSD values (Fig. 8, (a)). Conformational differences are detected between the crystallographic structure and the MD structures (Supporting information, Fig. SI6, (c)). In the presence of the heme cofactor, the conformation of the N-terminal part is close to α-helix D, leading to a more compact protein. (Fig. 8, (c)) Hydrogen bonds (1.3 ± 1.0) are established between the two fragments (Fig. 8, (b)). Consequently to this compact

conformation, few hydrogen bonds are observed between the N-terminal fragment and the solvent (45.5 ± 4.8). Contrarily, in the simulated apo-enzyme, the loop extends from the enzyme into the solvent (Fig. 8, (c)). Thus, few hydrogen bonds (0.7 ± 0.9) are observed between the N-terminal extremity and the DE-fragment (Fig. 8, (b)) but more hydrogen bonds are established between the solvent and this part of the JK-loop (55.5 ± 4.2). Conformation variability of the N-terminal extremity may be essential for the protein. With this simultaneous opening of the C-terminal and the N-terminal extremities in absence of the cofactor, the protein pocket B is open and allows a free heme cofactor to enter in the active site. Consequently, the N-terminal part of the loop regulates hIDO1 activity. Similar hypothesis is consistent with the heme lability and the incorporation of a L-Trp in the inhibitor site in absence of the heme cofactor. At last, independently from the presence or the absence of the cofactor, the N-terminal extremity involves the folding of residues E369 to E375 into a short helix stabilized by an increased number of hydrogen bonds (Fig. 8, (d)). This folding (Fig. 8, (d)) indicates the possible structural organization of the segment despite its flexibility.

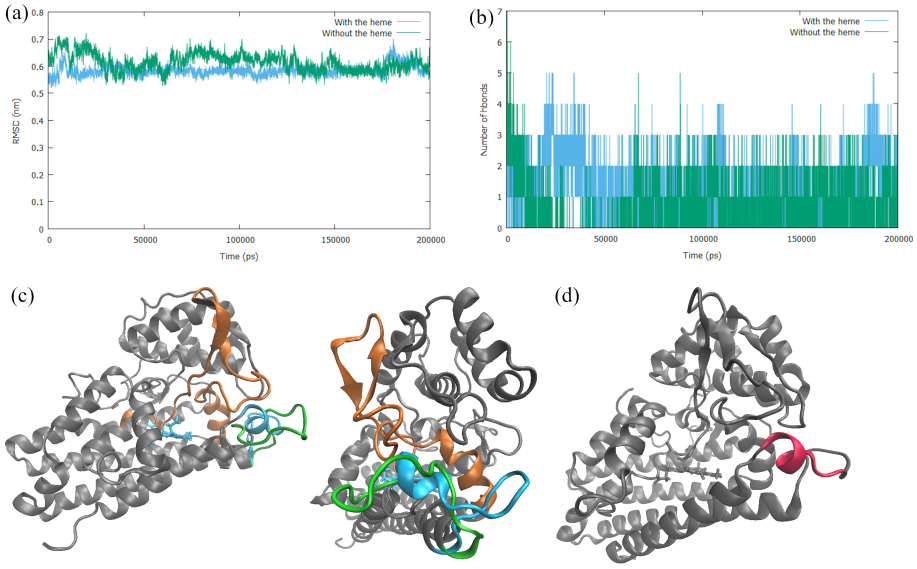

Fig. 8. Impact of the heme cofactor on the JK-loop conformation on the N-terminal part (with the cofactor (cyan), without the cofactor (green), DE-fragment is coloured in orange). (a) RMSD analysis of the N-terminal part (Q360-L374) of the JK-loop according to the cofactor occupancy. (b) Hydrogen bonds pairs (cut-off value of 3.5 Å and 30 degrees) analyses for residues Q360 to L374, per frame of 20 ps. (c) Conformation of N-terminal extremity according to the presence of heme cofactor with frontal view (left) and lateral view (right) as obtained from 200 ns of MD simulation at 300 K and 1 bar. (d) Conformation of helix between S369 to E375 (red) in simulation with heme cofactor as obtained from 200 ns of MD simulation at 300 K and 1 bar.

4. Conclusion

The hIDO1 crystal structure reported here contains four monomers in the asymmetric unit. For the first time, a complete refined JK-loop was determined in one of the monomers. The hIDO1 structure was refined at a resolution of 2.44 Å and the R_{work} and R_{free} are equal to 0.2118 and 0.2579, respectively with reasonable statistics (Ramachandran plot, rotamer analysis and r.m.s deviation values). The structure, which is mainly composed of two domains consisting of α and 3_{10} helices, is involved in multiple dimerization interfaces between the monomers within the asymmetric unit.

The refined conformation of the JK-loop adopts a new conformation between the

reported intermediate and the fully extended ones. Lysine K377, located at the C-terminal part of the loop, is involved in an electrostatic interaction with the heme cofactor. The N-terminal part of the loop is very flexible, this segment being associated with high B-factors values. As a result of the intermediate conformation of the loop, the active site of the enzyme forms a "pocket B" with a volume of 249 $\mathring{A}^3$. In the absence of a ligand, the JK-loop intermediate conformation of hIDO1, is seen to plays a crucial role in the regulation of the activity on the enzyme and/or the stable binding of the heme cofactor into the active site.

Through the analysis of Molecular Dynamic (MD) trajectories, the flexibility of the JK-loop was quantified by Root Mean Square Displacement (RMSD) and Root Mean Square Fluctuation (RMSF) profile analyses. Simulation with a potentially labile heme cofactor leads to a structure consistent with the crystal structure, the heme remaining stabilized by interactions with lysine K377. The simulated lack of a heme cofactor induces (1) an opening of the C-terminal extremity of the JK-loop, starting at K377 as indicated by the increase by a factor of 2 of the distance between A264 and K377 (2) a transfer of hydrogen bonds from the DE-fragment to the solvent molecules at the level of the N-terminal extremity. Regarding the N-terminal part of the JK-loop, a helix-type folding of residues E369 to E375, stabilised by an increased number of hydrogen bonds is observed, independently from the presence or the absence of the cofactor.

In conclusion, the experimental and MD results presented in the paper complete the data previously reported in literature on hIDO1 while stressing on the importance of the JK-loop conformation. This new combined information shows the importance of the JK-loop on the protein dynamics that occurs during catalysis and the importance of the conformation of the JK-loop in the absence of an other ligand to maintain a labile heme into the active site. The crucial role that the labile heme cofactor plays

and that was confirmed here deserves further biophysical studies that will benefit from the structural work disclosed in the present study.

Acknowledgements Authors are grateful from SOLEIL synchrotron for access to synchrotron radiation facilities and acknowledge PROXIMA I staff for assistance during the experiment and Serena Sirigu for the help during the indexation. Authors also thank Pr. Liang Tong for providing hIDO1 plasmid with surface mutations. This research used resources of the "Plateforme Technologique de Calcul Intensif (PTCI)" (http://www.ptci.unamur.be) located at the University of Namur, Belgium, which is supported by the FNRS-FRFC, the Walloon Region, and the University of Namur (Conventions No.2.5020.11, GEQU.G006.15, 1610468, and RW/GEQ2016). The PTCI is member of the "Consortium des Equipements de Calcul Intensif (CÉCI)" (http://www.ceci-hpc.be). The authors acknowledge the reviewers and the editor for the precious advices concerning the manuscript. M.Mirgaux acknowledges the Fonds de la Recherche Scientifique (F.R.S.-FNRS, Belgium) for her Research Fellow grant.

Contributions M. Mirgaux carried out the experiments, refined and analyzed the structure and took the lead for the manuscript redaction. Molecular Dynamics protocols were developed by M. Mirgaux and L. Leherte. Both authors contributed to the interpretation of the results. J. Wouters designed the project and supervised the work. All authors provided critical feedback and helped in the research, the analysis and the manuscript.

Funding This work was financed using by Fonds de la Recherche Scientifique (F.R.S.-FNRS, Belgium).

References

Abraham, M. J., Van der Spoel, D., Lindahl, E., Hess, B., & the GROMACS development team (2016). *GROMACS User Manual version 5.1.4.*

Adams, P. D., Afonine, P. V., Bunkóczi, G., Chen, V. B., Davis, I. W., Echols, N. , Headd, J. J., Hung, L-W, Kapral, G. J., & Grosse-Kunstleve, R. W. *et al.* (2010). *Acta. Cryst.*, D**66**(2), 213-221.

Alexandre, J. A. C., Swan, M. K., Latchem, M. J., Boyall, D., Pollard, J. R., Hughes, S. W., & Westcott, J. (2018). *Chembiochem*, **19**(6), 552-561.

Álvarez, L., Lewis-Ballester, A., Roitberg, A., Estrin, D. A., Yeh, S.-R., Marti, M. A., & Capece, L. (2016). *Biochemistry*, **55**(19), 2785-2793.

Badawy, A. (2017). *Int. J. Tryptophan Res.*, **10**, 1-20.

Birktoft, J. J., & Banaszak, L. J. (1983). *J. Biol. Chem.*, **258**, 472-482.

Bussi, G., Donadio, D., & Parrinello, M. (2007). *J. Chem. Phys.*, **126**(1), 014101.

Chen, V. B., Arendall, W. B., Headd, J. J., Keedy, D. A., Immormino, R. M., Kapral, G. J., Murray, L. W., Richardson, J. S., & Richardson, D. C. (2010). *Acta. Cryst.*, D**66**(1), 12–21.

Crosignani, S., Bingham, P., Bottemanne, P., Cannelle, H., Cauwenberghs, S., Cordonnier, M., Dalvie, D., Deroose, F., Feng, J. L., & Gomes, B. (2017). *J. Med. Chem*, **60**(23), 9617-9629.

Darré, L., Tek, A., Baaden, M., & Pantano, S. (2012). *J. Chem. Theory Comput.*, **8**(10), 3880–3894.

Emsley, P., Lohkamp, B., Scott, W. G., & Cowtan, K. (2010). *Acta. Cryst.*, D**66**(4), 486-501.

Gonzalez, H. C., Darré, L., & Pantano, S. (2013). *J. Phys. Chem. B*, **117**(46), 14438–14448.

Hess, B., Bekker, H., Berendsen, H. J., & Fraaije, J. G. (1997). *J. Comput. Chem.*, **18**(12), 1463-1472.

Hoffmann, D., Pilotte, L., Stroobant, V., & Van den Eynde, B. (2019). *Int. J. Tryptophan Res.*, **12**, 1-8.

Iwaoka, M., & Babe, N. (2015). *Phosphorus Sulfur. Silicon. Relat. Elem.*, **190**(8), 1257-1264.

Kabsch, W. (2010). *Acta Cryst.*, D**66**(2), 125–132.

Katz, J. B., Muller, A. J., & Prendergast, G. (2008). *Immunol. Rev.*, **222**(1), 206-221.

King, N. J.C., & Thomas, S. R. (2007). *Int. J. Biochem. Cell Biol.*, **39**(12), 2167-2172.

Kolodziej, L. R., Paleolog, E. M., & Williams, R. O. (2011). *J. Amino Acids*, **41**, 1173-1183.

Kumar, S., Waldo, J. P., Jaipuri, F. A., Marcinowicz, A., Van Allen, C., Adams, J., Kesharwani, T., Zhang, X., Metz, R., & Oh, A. J. *et al.* (2019). *J. Med. Chem.*, **62**(14), 6705-6733.

Leonardo, D., Machado, M. R., Brandner, A. F., Gonzalez, H. C., Ferreira, S., & Pantano, S. (2015). *J. Chem. Theory Comput*, **11**(2), 723–739.

Lewis-Ballester, A., Pham, K. N., Batabyal, D., Karkashon, S., Bonanno, J. B., Poulos, T. L., & Yeh, S.-R. (2017). *Nat Commun*, **8**, 1693.

Lewis-Ballester, A., Karkashon, S., Batabyal, D., Poulos, T. L, & Yeh, S.-R. (2018). *J. Am. Chem. Soc.*, **140**(27), 8518-8525.

Long, G. V., Dummer, R., Hamid, O., Gajewski, T. F., Caglevic, C., Dalle, S., Arance, A., Carlino, M. S., Grob, J.-J. & Kim, T. M. and others (2019). *The Lancet Oncology*, **20**(8), 1083-1097.

Luo, S., Xu, K., Xiang, S., Chen, J., Chen, C., Guo, C., Tong, Y., & Tong, L. (2018). *Acta. Cryst.*, F**74**(11), 717-724.

MacKerell Jr, A. D., Banavali, N., & Foloppe, N. (2000). *Biopolymers*, **56**(4), 257-265.

McCoy, A.J., Grosse-Kunstleve, R.W., Adams, P.D., Winn, M.D., Storoni, L.C., & Read, R.J. (2007). *J. Appl. Cryst.*, **40**(4), 658–674.

Mellor, A. L., & Munn, D. H. (2004). *Nat. Rev. Immunol.*, **4**, 762-774.

Mellor, A. L., Lemos, H., & Huang, L. (2017). *Front. Immunol.*, **8**:1360

Moon, Y. W., Hajjar, J., Hwu, P., & Naing, A. (2015). *J. Immunother. Cancer.*, **3**, 51.

Moriarty, N.W., Grosse-Kunstleve, R.W. & Adams., P.D. (2009). *Acta. Cryst.*, D**65**, 1074-1080.

Munn, D. H., & Mellor, A. L. (2007). *J. Clin. Invest.*, **117**(5), 1147-1154.

Munn, D. H., & Mellor, A. L. (2013). *Trends. Immunol.*, **34**(3), 137-143.

Munn, D. H., & Mellor, A. L. (2016). *Trends. Immunol.*, **37**(3), 193-207.

Nelp, M. T. and Kates, P. A., Hunt, J. T., Newitt, J. A., Balog, A., Maley, D., Zhu, X., Abell, L., Allentoff, A., & Borzilleri, R. *et al.* (2018). *P. Natl. Acad. Sci. USA.*, **115**(13), 3249-3254.

Nienhaus, K. ,& Nienhaus, G. U. (2018). *Front. Mol. Biosci.*, **4**,94.

Pal, D., & Chakrabarti, P. (2001). *J. Biomol. Struct. Dyn*, **19**(1),115-128.

Parrinello, M., & Rahman, A. (1981). *J. Appl. Phys.*, **52**(12), 7182-7190.

Peng, Y.-H., Ueng, S.-H., Tseng, C.-T., Hung, M.-S., Song, J.-S., Wu, J.-S., Liao, F.-Y., Fan, Y.-S., Wu, M.-H., & Hsiao, W.-C. *et al.* (2016). *J. Med. Chem*, **59**(1), 282-293.

Peng, Y.-H., Liao, F. Y., Tseng, C. T., Kuppusamy, R., Li, A. S., Chen, C. H. *et al.* , & Hsiao, W.-C. (2020). *J. Med. Chem*, **63**(4), 1642-1659.

Pham, K. N., & Yeh, S.-R. (2018). *J. Am. Chem. Soc*, **140**,(44), 14538-14541.

Pham, K. N., Lewis-Ballester, A., & Yeh, S.-R. (2019). *J. Am. Chem. Soc*, **141**(47), 18771-18779.

Phillips, R. S., Iradukunda, E. C., Hughes T., & Bowen, J. P. (2019). *Front. Mol. Biosci.*, **6**, 3.

Prendergast, G. C. (2008). *Oncogene*, **27**, 3889-3900.

Prendergast, G. C., Malachowski, W. J., Mondal, A., Scherle, P., & Muller, A. J. (2018). *Int. Rev. Cel. Mol. Bio.*, **336**, 175-203.

Raven, E. L. (2017). *J. Biol. Inorg. Chem.*, **22**, 175-183.

Rohrig, U. F., Reynaud, A., Majjigapu, S. R., Vogel, P., Pojer, F., & Zoete, V. (2019). *J. Med. Chem.*, **62**(19), 8784-8795.

Schrödinger, LLC (2010). *The PyMOL Molecular Graphics System, Version 1.8.*

Shahrokh, K., Orendt, A., Yost, G. S., & Cheatham, T. E (2012). *J. Comput. Chem.*, **33**,(2) 119-133.

Shankar, B. G., Sarani, R., Michael, D., Mridula, P., Ranjani, C. V., Sowmiya, G., & Seka, K. *et al.* (2007). *J. Biosci.*, **32**, 693-704.

Sugimoto, H., Oda, S.-I., Otsuki, T., Hino, T., Yoshida, T., & Shiro, Y. (2006). *P. Natl. Acad. Sci. USA.*, **103**(8), 2611-2616.

Takikawa, O. (2005). *Biochem. Biophys. Res. Commun.*, **338**(1), 12-19.

Terwilliger, T.C, Read, R. J., Adams, P. D., Brunger, A. T., Afonine, P. V., Grosse-Kunstleve, R. W. & Hung, L. W. (2012). *Acta Crystallogr D Biol Crystallogr*, D**68**(7), 861-870..

Tojo, S., Kohno, T., Tanaka, T., Kamioka, S., Ota, Y., Ishii, T., Kamimoto, K., Asano, S., & Isobe, Y. (2014). *ACS. Med. Chem. Lett.*, **5**(10), 1119-1123.

Uyttenhove, C., Pilotte, L., Théate, I., Stroobant, V., Colau, D., Parmentier, N., Thierry, B., & Van den Eynde, B. J. (2003). *Nat. Med.*, **9**, 1269-1274.

White, C., McGowan, M. A., Zhou, H., Sciammetta, N., Fradera, X., Lim, J.,*et al.*, & Trewick, S. (2020). *ACS Med. Chem. Lett*, **11**(4) 550-557.

Wu, Y., Xu, T., Liu, J., Ding, K., & Xu, J. *et al.* (2017). *Biochem. Biophys. Res. Commun.*, **487**(2), 339-343.

Yu, J., Zhou, Y., Tanaka, I., & Yao, M. (2010). *Bioinformatics*, **26**(1), 46-52.

Zhang, H., Liu, K., Pu, Q., Achab, A., Ardolino, M. J., Cheng, M., Deng, Y., Doty, A. C., Ferguson, H., & Fradera, X. *et al.* (2019). *ACS Med. Chem. Lett.*, **10**(11), 1530-1536.

Synopsis

This article consists of a in-deep analysis of structural aspects for the heme-bound structure of hIDO1 with a complete refined JK-loop (overall crystal structure, quality of the structure, dimerization interfaces, and analysis of the JK-loop conformation) followed by a Molecular Dynamics study of the influence of the heme occupation on the JK-loop conformation.

Influence of the presence of the heme cofactor on the JK-loop structure in indoleamine-2,3-dioxygenase-1: Supporting information

1. Type of conformation for JK-loop in the C-terminal part from literature

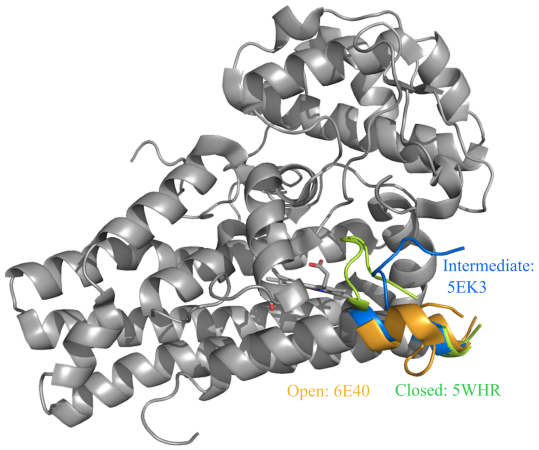

Fig. SI1. Conformation of the C-terminal part for the JK-loop in the literature. (a) Closed conformation from 5WHR (green) (b) Intermediate conformation from 5EK3 (blue) (c) Open conformation from 6E40 (orange).

2. Solvatation in Molecular Dynamic simulation

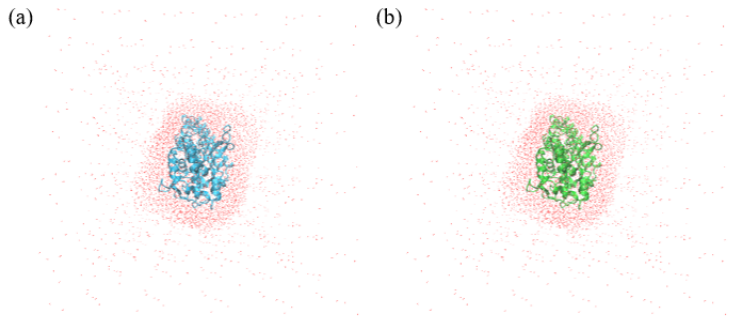

Fig. SI2. All-atom water solvent in each simulation. (a) Simulation with the heme cofactor. (b) Simulation without the heme cofactor.

3. Dimerization interface

Table SI1. *Distances involved in dimeric interaction in the small unit from Fig. 4.*

Dimerisation interface	Monomer	Amino acids (atoms)	Monomer	Amino acids (atoms)	Distances (Å)
P104-E119	A	D68 (OD2)	D	M64 (SD)	3.9
	A	M64 (SD)	D	D68 (OD1)	3.8
	A	M64 (SD)	D	D68 (OD2)	3.6
	A	D68 (OD2)	D	R105 (NH2)	3.9
	A	Q113 (NE2)	D	Q113 (OE1)	3.8
	A	Q113 (OE1)	D	Q113 (NE2)	3.9
	A	K257 (NZ)	D	E119 (OE1)	3.6
	A	K257 (NZ)	D	E119 (OE2)	3.6
Y36-H45	A	N37 (OD1)	D	R58 (NH2)	2.6
and Q54-K61	A	D38 (OD1)	D	W609 (O)	2.7
	D	W609 (O)	D	R58 (NH2)	3.6
	D	W609 (O)	D	Q54 (OE1)	2.3
	D	W608 (O)	D	R58 (NH1)	2.3
	D	W608 (O)	D	E57 (OE2)	2.9
	D	R58 (NH1)	D	E57 (OE2)	4.2
	A	R58 (NH1)	D	E57 (OE1)	2.9
	A	R58 (NH1)	D	E57 (OE2)	3.4
	A	R58 (NH2)	D	E57 (OE1)	2.3
	A	R58 (NH2)	D	E57 (OE2)	3.5
	D	E57 (OE1)	D	K61 (NZ)	3.0

Table SI2. *Distance involved in dimeric interaction in the large unit from Fig. 5.*

Dimerization interface	Monomer	Amino acids (atoms)	Monomer	Amino acids (atoms)	Distances (Å)
Helix D	A	D219 (OD1)	A	W613 (O)	2.4
	A	D219 (OD1)	A	W745 (O)	3.7
	A	D219 (OD2)	A	W745 (O)	3.8
	A	D219 (OD1)	A	W735 (O)	2.4
	A	W745 (O)	D	W735 (O)	3.4
	A	W745 (O)	D	W718 (O)	2.2
	D	W718 (O)	D	H220 (O)	3.6
	A	D219 (OD2)	D	W621 (O)	3.5
	D	W612 (O)	D	W718 (O)	3.6
	A	W612 (O)	D	H218 (O)	2.4
	A	W612 (O)	D	E146 (OE2)	3.2
	A	W612 (O)	D	H220 (NE2)	3.2
	D	W614 (O)	D	E146 (OE1)	2.4
	D	W614 (O)	D	E146 (OE2)	2.6
	D	W614 (O)	D	W732 (O)	2.4
	D	W614 (O)	D	W603 (O)	2.5
	D	W603 (O)	D	H220 (NE2)	3.8
	A	H218 (NE2)	D	D219 (OD1)	3.8
	A	H218 (ND1)	D	D219 (OD2)	4.0
	A	H218 (ND1)	D	D219 (OD1)	4.1
	A	H218 (NE2)	D	D219 (OD2)	4.9
BC-loop and HI-loop	A	R193 (NH1)	A	D325 (OD1)	2.8
	A	R193 (NH1)	A	D325 (OD2)	3.3
	A	R193 (NE)	A	D325 (OD2)	2.7
	A	D325 (OD2)	C	R193 (NE)	4.7
	A	Q191 (OE1)	C	K323 (NZ)	4.1
	A	K323 (NZ)	C	Q191 (OE1)	4.3
	C	K323 (NZ)	C	Q191 (OE1)	4.1
	C	D325 (OD2)	C	R193 (NH1)	3.4
	C	D325 (OD1)	C	R193 (NH1)	2.9
	C	D325 (OD2)	C	R193 (NE)	2.7

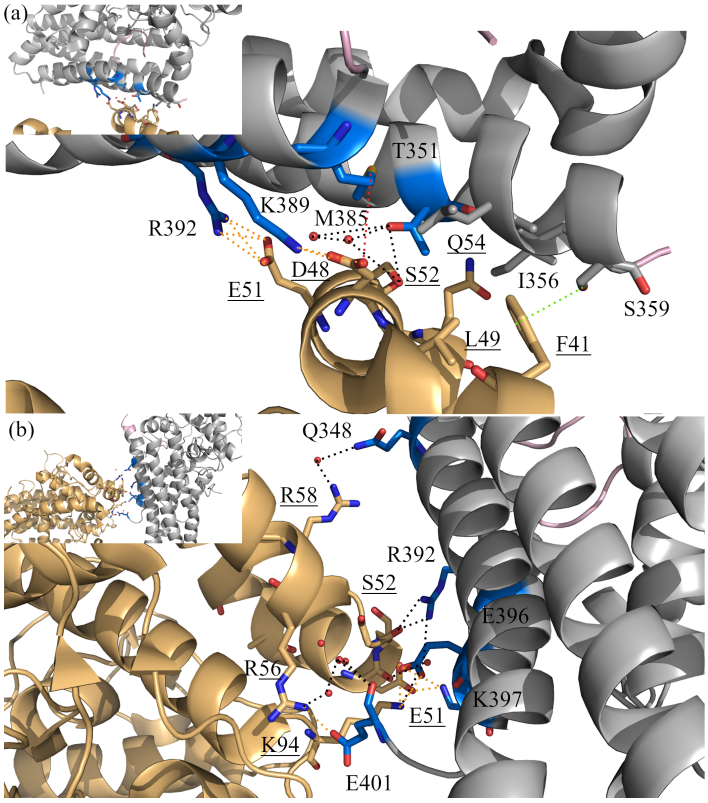

Fig. SI3. Dimerization interfaces in 5WHR around the JK-loop. (a) Interface with the α-helix H45-S52 (b) Interface with the α-helix Q54-K61.

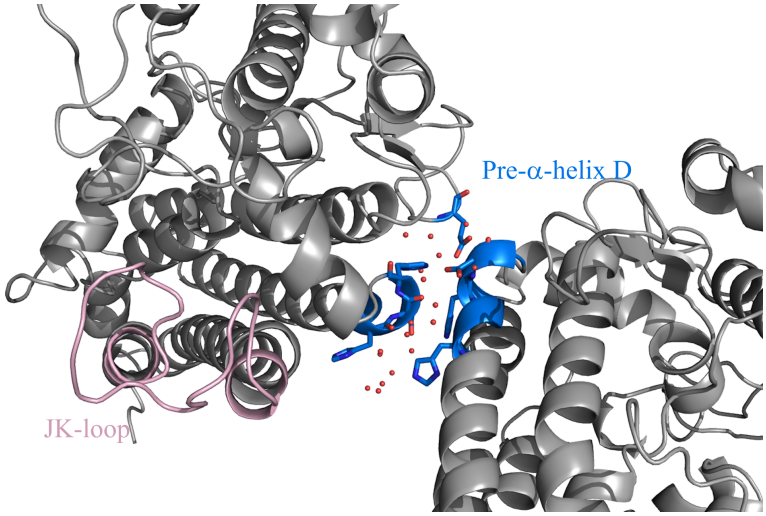

Fig. SI4. Dimerization interface of the α-helix D (in blue) in relation to the JK-loop (in pink).

4. Conformation of JK-loop in 7A62

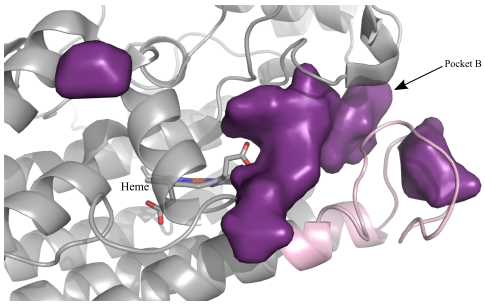

Fig. SI5. Volume of the pocket B resulting of the JK-loop conformation. Cavity was generated by POCASA 1.1. server (Yu, J. *et al.*, 2010).

5. Link between JK-loop conformation and heme lability supported by Molecular Dynamics

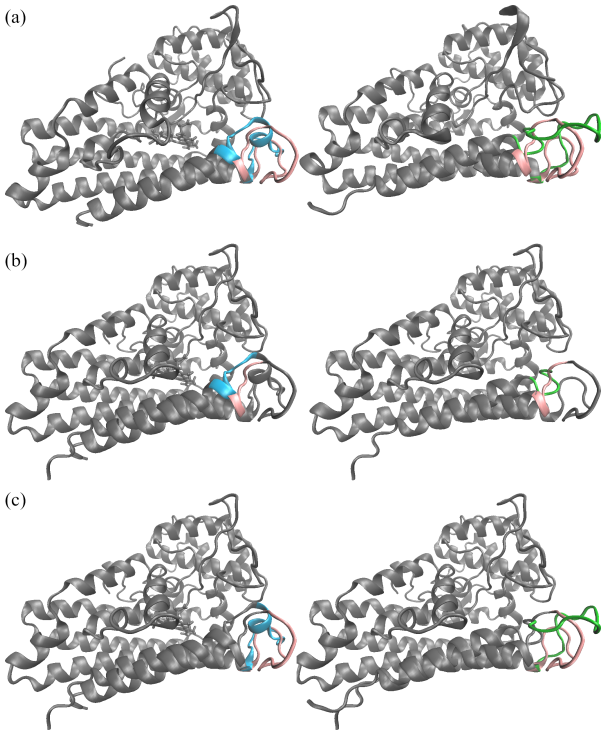

Fig. SI6. Superimposition of the crystal (pink), MD simulation with the heme cofactor at t = 200 ns (cyan), and MD simulation structure without the heme cofactor at t = 200 ns (green) (a) Overall view (b) C-terminal part of the JK-loop (E375 to G380) (c) N-terminal part of the JK-loop (Q360 to E374).

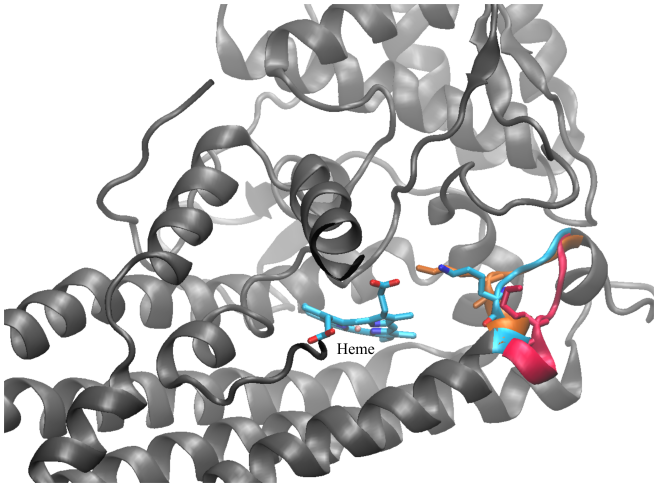

Fig. SI7. Superimposition of different locations for K377 obtained from the MD simulation with the heme cofactor. Conformations are clustered in three groups: closed (in orange, the distance between K377 and A264 varies from 6 Å to 10 Å, 16.1% of the conformations), intermediate (in cyan, the distance between K377 and A264 varies from 10 Å to 16 Å, 79.3% of the conformations) and open (in red, the distance between K377 and A264 is larger than 16 Å, 4.6% of the conformations). Percentages were calculated over a 200 ns MD simulation at 300 K and 1 bar.

References

Yu, J., Zhou, Y., Tanaka, I., & Yao, M. (2010). *Bioinformatics*, **26**,(1) 46-52.